Magnetic and Orbital Order in $LaMnO_3$ under Uniaxial Strain: A Model Study

B. R. K. Nanda and S. Satpathy
Department of Physics, University of Missouri, Columbia, Missouri 65211, USA
(Dated: November 5, 2009)

The effect of uniaxial strain on electronic structure and magnetism in $LaMnO_3$ is studied from a model Hamiltonian that illustrates the competition between the Jahn-Teller, super exchange, and double exchange interactions. We retain in our model the three main octahedral distortions (Q_1, Q_2, and Q_3), which couple to the Mn (e_g) electrons. Our results show the ground state to be a type A antiferromagnetic (AFM) insulating state for the unstrained case, consistent with experiments. With tensile strain (stretching along the c axis), the ground state changes into a ferromagnetic and eventually into a type G′ AFM structure, while with compressive strain, we find the type A switching into a type G structure. The orbital ordering, which displays the well known checkerboard x^2-1/y^2-1 structure for the unstrained case, retains more or less the same character for compressive strain, while changing into the z^2-1 character for tensile strains. While Q_1 and Q_3 are fixed by the strain components ε_{xx} and ε_{zz} in our model, the magnitude of the in-plane distortion mode (Q_2), which varies to minimize the total energy, slowly diminishes with tensile strain, completely disappearing as the FM state is entered. Within our model, the FM state is metallic, while the three AFM states are insulating.

PACS numbers: 75.47.Lx; 75.10.-b; 71.70.Ej

I. INTRODUCTION

It is well known that the interplay between the orbital, lattice, and spin degrees of freedom in the lanthanum manganite, a key member of the colossal magnetoresistive materials, produces a checkerboard orbital-ordered ground state by the cooperative Jahn-Teller effect and simultaneously the type A antiferromagnetic ordering. However, a detail knowledge of what happens to this ground state under the application of strain or uniform pressure is lacking.

On the other hand, high-quality, lattice-matched heterostructures of the manganites have begun to be grown and studied, heterostructures that are frequently under uniaxial strain due to the pseudomorphic growth condition during epitaxial growth. The variation of layer thickness and substrate induce different magnetic ground states ranging from complete ferromagnetic ordering to a canted magnetic state or an antiferromagnetic state[1,2,3,4,5]. An interesting two-dimensional spin-polarized electron gas was also predicted for the manganite heterostructures.[6] In addition, the magnetotransport studies on bulk $LaMnO_3$(LMO) under pressure[7,8,9,10] and LMO thin films grown on different substrates[11,12,13,14,15,16,17] show metal insulator transitions accompanied by magnetic transitions. Theoretically, it is known that strain can change orbital ordering in LMO, which affects magnetism,[18] and leads to modified properties in the manganite superlattices.[19,20] The commonalities involved in these are strain, either induced by pressure or due to substrate.

It is therefore important to understand the ground-state of the underlying material, viz., the bulk LMO under uniaxial strain condition. It is the goal of the paper to provide this insight by studying a simple model Hamiltonian that contains the relevant interactions important for this material.

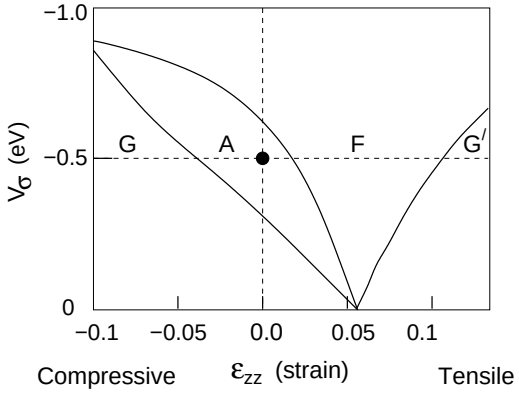

FIG. 1: The ground-state magnetic phase diagram for LMO as a function of strain and the $dd\sigma$ electronic hopping V_σ, as obtained from our model. Type A represents the phase with ferromagnetic ab planes stacked antiferromagnetically along the c axis, while F and G stand, respectively, for the ferromagnetic and the Neél ordered antiferromagnetic state. We distinguish between two type G states (G and G′) depending on the orbital occupancy of the Mn e_g electron: x^2-1 or y^2-1 for G and z^2-1 for G′. For LMO, V_σ is about -0.5 eV.

Density-functional studies[21,22,23,24] of the unstrained LMO have provided important insights into the physics of the system regarding how the Jahn-Teller (JT) coupling, orbital ordering, and magnetism are intertwined. The few such studies performed for the strained LMO are focused on the uniform pressure situation and indeed they do find changes in the magnitude of the JT distortions as well as in the conduction properties.[25,26] Above the critical pressure of 32 GPa, LMO becomes metallic and the JT distortion appears to be completely suppressed.[8,9] Systematic experimental work as well as theory work on the uniaxial strain situation is missing; yet, as already

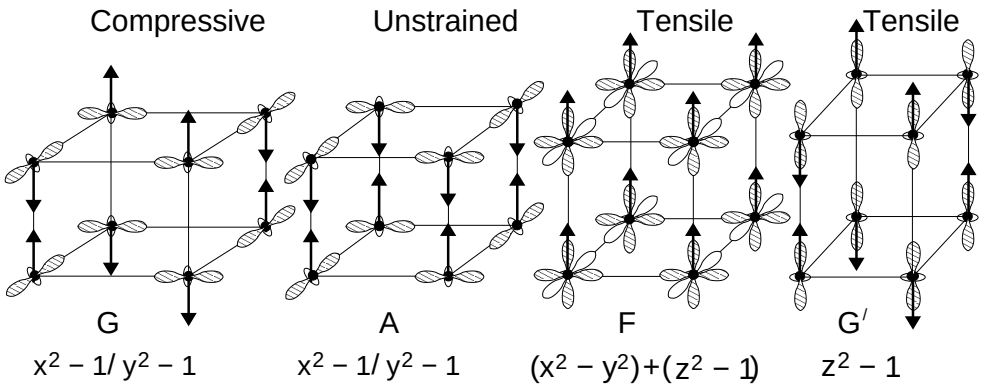

FIG. 2: The magnetic and orbital order of the four phases under varying strain conditions as obtained from our model. Shown are only the Mn atoms and arrows denote the t_{2g} core spins. Tensile strain means stretching along the c direction, normal to the ab plane.

mentioned, this strain condition is frequently realized in thin films and superlattices grown on different substrates and must be understood before an understanding of the superlattices of LMO can be accomplished.

In this paper, we study the interplay between the lattice, orbital, and magnetic degrees of freedom in LMO under uniaxial strain condition by using a tight-binding model that includes the relevant interactions, viz., the antiferromagnetic super exchange between the t_{2g} core spins, the double exchange between the core spins and the itinerant e_g electrons, the electronic band structure energy, as well as the JT coupling between the e_g electrons and the lattice.

At this stage, a model study is more instructional than a density-functional study, since unlike the latter, one can vary here the relative strengths of the various interactions and study their effect on the ground state, providing us with valuable insight into the system. This study will be important in understanding the experimental results on strained LMO as well as help interpret results of detail *ab initio* calculations, which are in progress and will be reported elsewhere.[27]

Our results, summarized in Figs. 1 and 2, show that the magnetic state, the JT distortions, the orbital ordering, as well as conduction properties, all change with uniaxial strain. As strain changes from compressive to tensile, the system changes from a type G antiferromagnetic (AFM) to the type A AFM phase, then to a ferromagnetic phase (F), ultimately changing into a type G′ phase. The FM phase is metallic, while the rest are insulating phases. As regards the orbital ordering, while the unstrained LMO shows the well known checkerboard $x^2 - 1/y^2 - 1$ ordering on the ab plane, the application of compressive strain retains the same orbital structure more or less, while tensile strain results in a $z^2 - 1$ orbital ordering. As the strain is changed from compressive to tensile, the magnitude of the in-plane distortion (Q_2 mode) diminishes, eventually disappearing completely for the ferromagnetic phase and beyond. The changes in the various features are intertwined with one another as discussed below.

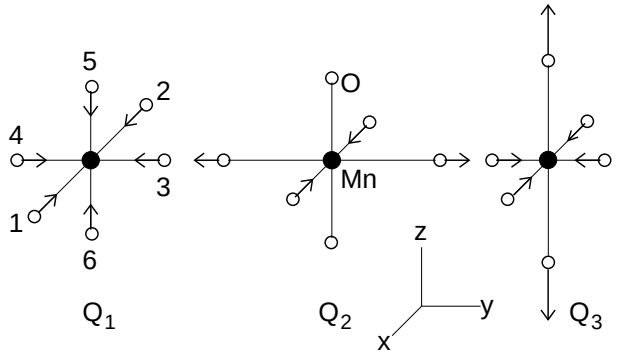

FIG. 3: Vibronic modes for the MnO_6 octahedron with the eigenvectors: $|Q_1\rangle = (-X_1 + X_2 - Y_3 + Y_4 - Z_5 + Z_6)/\sqrt{6}$, $|Q_2\rangle = (-X_1 + X_2 + Y_3 - Y_4)/2$, and $|Q_3\rangle = (-X_1 + X_2 - Y_3 + Y_4 + 2Z_5 - 2Z_6)/\sqrt{12}$, where X_1 denotes the x coordinate of the first oxygen atom, etc.

II. THE MODEL HAMILTONIAN

We consider the following model Hamiltonian, restricted to the Mn sites in a tetragonal lattice, with lattice constants being different along the plane and normal to the plane in order to accommodate the uniaxial strain:

$$\mathcal{H} = \sum_i \frac{1}{2} K {Q_i}^2 + \sum_i \mathcal{H}^i_{JT} + \mathcal{H}_{ke} + \frac{J}{2} \sum_{<ij>} \vec{S}_i \cdot \vec{S}_j, \quad (1)$$

where i is the site index and $< ij >$ denotes summation over nearest-neighbor sites. The last term describes the antiferromagnetic superexchange interaction between the Mn t_{2g} spins, treated as classical, which provide the background for the motion of the itinerant Mn e_g electrons. The first two terms in the Hamiltonian describe the Jahn-Teller interaction of the Mn e_g electrons with the lattice, where the first term is the elastic energy with

$Q^2 = Q_1^2 + Q_2^2 + Q_3^2$, with Q_1 being the breathing mode, Q_2 being the basal plane distortion mode, and Q_3 being the octahedral stretching mode as shown in Fig. 3. These are the three important modes that couple to the e_g electrons.

The JT interaction at each Mn site is given by[28]

$$\begin{aligned}\mathcal{H}_{JT} &= g'Q_1 I - g(Q_3\tau_z + Q_2\tau_x) \\ &\quad -G(Q_3^2 - Q_2^2)\tau_z + 2GQ_2Q_3\tau_x, \end{aligned} \tag{2}$$

where both the linear and quadratic vibronic couplings are included. The quadratic coupling is necessary to describe the checkerboard orbital ordering on the ab plane.[29] In Eq. 2, $\vec{\tau}$ is the pseudospin describing the two e$_g$ orbitals, viz., $|\uparrow\rangle = |z^2 - 1\rangle$ and $|\downarrow\rangle = |x^2 - y^2\rangle$. Denoting the creation operators for these two orbitals on the i-th site by $c_{i1}^\dagger$ and $c_{i2}^\dagger$, respectively, the pseudospin operator at the i-th site in Eq. 2 is written as: $\vec{\tau}_i = \sum_{\alpha\beta} c_{i\alpha}^\dagger \vec{\tau}_{\alpha\beta} c_{i\beta}$, where the greek indices denote the orbitals and i is the site index. The lattice interactions do not depend on the electron spin, which therefore does not appear in Eq. 2.

The kinetic energy term in the Hamiltonian may be written as

$$\mathcal{H}_{ke} = \sum_{\langle ij\rangle,\alpha\beta} t_{i\alpha,j\beta}\cos(\theta_{ij}/2) c_{i\alpha}^\dagger c_{j\beta} + H.c., \tag{3}$$

where the value of the Hund's energy is taken as $J_H = \infty$. In this limit, the coupling between the core and the itinerant spins, $\mathcal{H}_{Hund} = -J_H \sum_{i\alpha} \vec{S}_i \cdot \vec{s}_{i\alpha}$, makes the electron state with the spin anti-aligned with the t_{2g} core spin at that site inaccessible to the system (core t_{2g} spin and the electron spin at the i-th site are denoted by $\vec{S}_i$ and $\vec{s}_i$ respectively). Thus the itinerant electrons are effectively described as spinless, with only its spin state aligned parallel to the core spin at a particular site being accessible to the system. The electron hopping is diminished by the well known Anderson-Hasegawa $\cos(\theta_{ij}/2)$ factor, where θ_{ij} is the angle between the core spins at the two sites.[30,31]

The nearest-neighbor (NN) hopping integral t depends on the relative positions of the two Mn sites. For NN along $\hat{x}$ or $\hat{y}$, we have[32]

$$t_{\alpha\beta} = \begin{pmatrix} 1 & -\sqrt{3} \\ -\sqrt{3} & 3 \end{pmatrix} \times \frac{V_\sigma}{4}, \tag{4}$$

while along $\hat{z}$, we have $t_{\alpha\beta} = \delta_{\alpha 1}\delta_{\beta 1} V_\sigma$, where V_σ is the $dd\sigma$ hopping parameter and we have neglected the much smaller $dd\delta$ interaction. The typical values of the Hamiltonian parameters used in our calculations throughout, unless otherwise stated, are: K = 9 eV/Å^2 following from the optical studies on $La_{0.85}Sr_{0.15}MnO_3$[33], g = 2.5 eV/Å, G = 1.5 eV/Å^2 and V$_\sigma$ = -0.5 eV following earlier density-functional results.[29] The value of the exchange energy is taken as $J = 26.2$ meV, which is the experimental value for $CaMnO_3$,[34,35] which has the $t_{2g}^3 e_g^0$ electronic configuration. Note that in our model Hamiltonian, g$'$ is an unimportant parameter, as it affects the energies of both the e_g orbitals equally and therefore adds a constant to the total energy.

We have considered the typical magnetic ordering of the core spins found in the manganites, viz., the A, C, G, and F types of magnetic states. Type C was always found to be of higher energy within our model. To accommodate these structures, the unit cell in the lattice consisted of four Mn atoms. The total energy was calculated by diagonalizing the Hamiltonian (1) and adding the energies of the occupied states in the Brillouin zone, corresponding to one e_g electron per Mn atom, for the various strain conditions and magnetic configurations.

Strain and the JT parameters – In our model, since we keep only the three main octahedral modes, the strain components are related to the magnitudes of the JT distortions. We consider only uniaxial strain conditions but no shear, so that only the diagonal components of the strain tensor are non zero.

For the unstrained crystal, the ground-state in our model has a tetragonal lattice structure with type A magnetic configuration and a checkerboard JT distortion and orbital ordering. The JT distortion has been shown[29] to lead to the checkerboard distortions on the ab plane of the type (Q_2, Q_3) alternating with (-Q_2, Q_3) consistent with the experiments.

This checkerboard JT distortion in our model results in a tetragonal structure with the lattice constants being $a = \sqrt{2/3}\, Q_{10} - Q_{30}/\sqrt{3}$ and $c = a + \sqrt{3}\, Q_{30}$, where the zero in the subscript denotes the calculated magnitudes for the unstrained LMO. The magnitudes of these distortions that minimize the ground-state energy clearly depends on the Hamiltonian parameters used in the model. For our typical parameters, we find that $Q_{20} \approx 0.32$ Å and $Q_{30} \approx -0.18$ Å, which are close to the experimental values of 0.28 Å and -0.10 Å, respectively.[36] Optimization of Q_1 for the Hamiltonian yields, trivially, the result that $Q_{10} = -g'/K$, while the cell volume is given by $a^2 c \approx (\sqrt{2/3}\, Q_{10})^3$. So, in essence, the experimental volume of LMO, which corresponds to $Q_{10} = 4.85$ Å determines the ratio of $-g'/K$.

We note that c and a are independent of the strength of the in-plane distortion Q_2. Therefore, any strain that changes c and a will directly affect the Q_1 and Q_3 distortions only, whereas the system will have an optimized Q_2 distortion in order to achieve the minimum in the ground state energy. This is consistent with the experimental studies of bulk LMO under pressure, where it has been found that the Mn-O bond length along the c-axis changes linearly with the lattice parameter of the LMO unit cell, while the Mn-O bond lengths along the plane follow a non-linear behavior.[8,9]

Now, with uniaxial strain, the lengths of the axes become $a\,(1+\varepsilon_{xx})$ and $c\,(1+\varepsilon_{zz})$, respectively. The strain parameters completely determine the magnitudes of the

breathing and the octahedral stretching modes, viz.,

$$\begin{aligned} Q_1 &= Q_{10}(1 + 2\varepsilon_{xx}/3 + \varepsilon_{zz}/3) \\ Q_3 &= Q_{30}(1 + \varepsilon_{zz}) + \sqrt{2}Q_{10}(\varepsilon_{zz} - \varepsilon_{xx})/3. \end{aligned} \quad (5)$$

In addition, the Poisson's ratio ν relates the two strain components,[37] $\varepsilon_{xx} = (2\nu)^{-1}(\nu - 1)\varepsilon_{zz}$, so that there is a single strain parameter ε_{zz} in the problem. Rewriting Eq. (5) in terms of this parameter, we have

$$\begin{aligned} Q_1 &= Q_{10}(1 + \frac{2\nu - 1}{3\nu}\varepsilon_{zz}) \\ Q_3 &= Q_{30}(1 + \varepsilon_{zz}) + Q_{10}\frac{\sqrt{2}}{3}\frac{\nu + 1}{2\nu}\varepsilon_{zz}, \end{aligned} \quad (6)$$

so that in our model, the strain parameter fixes the values of the Q_1 and the Q_3 distortions. The magnetic configurations and the in-plane JT distortion Q_2 are then determined so as to minimize the total energy.

The value $\nu = 1/2$ corresponds to conservation of volume under strain and the measured values for materials are not too far from this. For the manganites, the measured value is $\nu \approx 0.4$,[37,38] which we use in our calculations together with the unstrained distortions $Q_{10} = 4.85$ Å and $Q_{30} = -0.18$ Å as indicated above. For the case of conserved volume ($\nu = 1/2$), the value of Q_1 does not change with strain, while for $\nu = 0.4$ and $\varepsilon_{zz} = 5\%$, it changes by less than a percent from Q_{10}, while Q_3 changes significantly. Furthermore, because of the form of the Hamiltonian, Eqs. (1) and (2), Q_1 adds just an elastic energy and shifts the energies of both components of the e_g orbitals uniformly, irrespective of the magnetic structure of the Mn core spins, so that the relative energies of the different magnetic structures for a given strain ε_{zz} are not affected by Q_1. Thus in essence Q_3 remains the sole parameter in the problem for obtaining the ground states for different strains and the two parameters ε_{zz} and Q_3 can be used interchangeably to describe the strain condition. It has been recently shown that for manganites, the strain parameter ε_{zz} can be varied by as much as $\pm 5\%$ by using different materials as substrates.[37]

III. RESULTS AND DISCUSSIONS

Isolated octahedra under strain – To begin on familiar grounds, we consider the situation where the intersite hopping integral $V_\sigma = 0$ in the Hamiltonian (1). This is equivalent to a collection of isolated MnO_6 JT centers, each under the applied strain condition. The octahedra interact only via the super exchange interaction of the Mn core spins that results in the Neél AFM order, but the orbital occupancy and the JT distortions are determined by the interaction within a single octahedron. We see from Fig. 1 that in this case the magnetic ordering changes from type G AFM to type G′ AFM beyond a certain value of tensile strain. This can be easily understood as explained below.

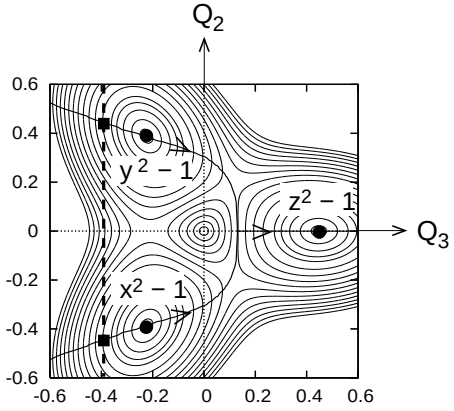

FIG. 4: Energy contours of an isolated Jahn-Teller center on the $Q_2 - Q_3$ plane with linear and quadratic coupling. The three global minima are indicated by the circular dots along with the corresponding occupied orbital; one of the three minima is occupied in the isolated octahedron. For the octahedron in the solid, the strain parameter ε_{zz} fixes the magnitude of Q_3 and the octahedron occupies the state marked by the square dots. As Q_3 is changed, the system traverses along the lines marked by the arrows. Beyond a critical value of the tensile strain (i.e., a critical Q_3), the orbital order abruptly switches from $x^2 - 1$ or $y^2 - 1$ like to $z^2 - 1$, making thereby a transition from G to G′ state.

The energy of an isolated octahedron, with one e_g electron occupied, is well known.[39] The expression is

$$E = \frac{1}{2}KQ^2 - Q(g^2 + G^2Q^2 + 2gG\cos(3\phi))^{\frac{1}{2}}, \quad (7)$$

where $Q = \sqrt{Q_2^2 + Q_3^2}$ and $\phi = \tan^{-1}(Q_2/Q_3)$. This leads to the energy contours with three equivalent minima at $\phi = 0, \pm 2\pi/3$ with $Q = g/(K - 2G)$ and the corresponding occupied orbital as shown in Fig. 4.

Now, when the octahedron is placed in LMO, the strain parameter ε_{zz} fixes the magnitude of Q_3 as given by Eq. (6), with the result that the state of the octahedron is given by minimizing the energy with respect to Q_2 only. The constrained minima for a certain value of Q_3 are shown by the square dots in Fig. 4. For the isolated octahedron, there are two equivalent minima with either the $x^2 - 1$ or the $y^2 - 1$ occupation; In the solid, they become staggered resulting in the checkerboard orbital order in the *ab* plane. As strain is changed, Q_3 changes and the system traverses along the lines marked by the arrows in the figure. Beyond a certain tensile strain, the strength of the Q_2 mode sharply reduces to zero, which is also accompanied by a transition in the orbital occupancy from $x^2 - 1$ or $y^2 - 1$ to $z^2 - 1$. The octahedra interact only via the super exchange term when the hopping term V_σ is zero, so that the Neél order is retained throughout, resulting in the transition from type G to G′ configuration as the orbital state changes.

Inter-octahedral hopping allowed – When the inter-octahedral hopping is allowed ($V_\sigma \neq 0$), it leads to a

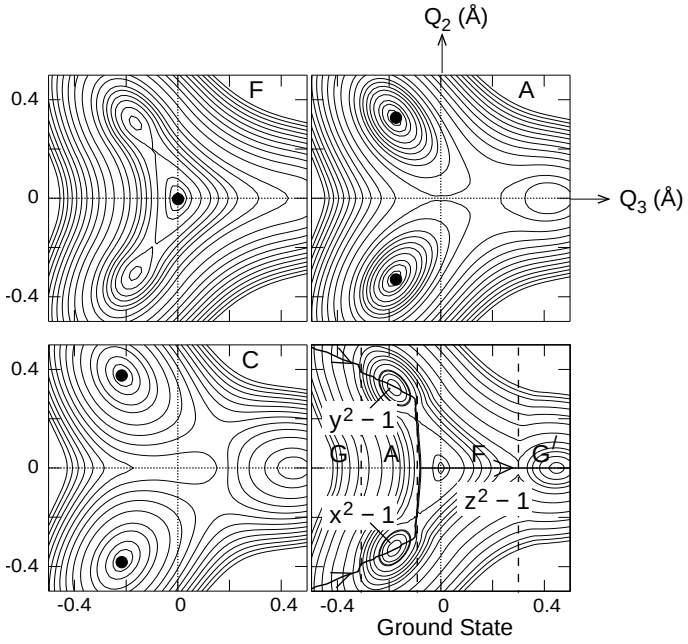

FIG. 5: Energy contours for different phases and for the minimum-energy phase (bottom right). For a fixed strain (fixed Q_3), the global minimum is obtained by varying Q_2 for each phase and comparing the minima thus obtained for each phase. The line with arrows indicates the state of the system as strain is varied. As strain changes from compressive to tensile, the magnetic state changes from G →A →F → G′, the magnitude of Q_2 slowly diminishes eventually becoming zero, and finally the orbital order changes from x^2-1/y^2-1 to z^2-1 type. Contours are obtained by solving Hamiltonian Eq. (1) with the hopping parameter V_σ = -0.5 eV.

cooperative JT ordering, i.e., that the JT distortions of the neighboring octahedra are organized so as to optimize the various energy terms in the solid. The ground-state configuration is determined by a competition between (i) the electron kinetic energy, which would prefer no JT distortion and a FM alignment of the core spins, so that all e_g orbitals are aligned and the kinetic energy gain due to hopping is maximized, (ii) the on-site JT interaction that would prefer a large octahedral distortion, at the same time balancing the elastic energy cost, and (iii) the super exchange energy that prefers antiferromagnetic alignment between all neighboring spins. If the electronic hopping is taken as zero, there is no conflict between the last two terms and a Neél state (G or G′) results as discussed above, simultaneously maximizing the JT energy gain and as well as the super exchange term.

With the switching on of the hopping term, all three energies cannot be simultaneously optimized. The resulting competition leads to a staggered orbital order accompanied by a staggered JT distortion, where both Q_2 and Q_3 distortions occur at each site, with Q_2 changing sign on neighboring sites and the x^2-1 and y^2-1 orbitals alternately occupied. The system thus stabilizes in the orbital ordered type A AFM state[29].

When strain is applied, other magnetic phases compete, resulting in different ground-state structures as shown in Fig. 1. To gain insight into the possible phases in strained LMO, we have kept the staggered JT distortion and examined four possible magnetic ordering, viz., A, F, G, and C. In Fig. 5 we have shown the energy contours in the Q_3-Q_2 plane for the type F, type A, and type C magnetic ordering. Results for type G ordering remains the same as in Fig. 5, irrespective of the magnitude of the hopping integral, since the Anderson-Hasegawa cos $(\theta/2)$ factor makes the effective hopping to be zero anyway. For the ferromagnetic ordering, the e_g-e_g hopping is allowed in all the directions. It is the strongest when there is no JT splitting of the e_g orbitals. Therefore the global minimum for the ferromagnetic ordering occurs at the center of the Q_3-Q_2 plane as can seen from the energy contours of Fig. 5. As we deviate from the center, JT-splitting reduces the effect of the hopping due to the energy denominator, which therefore weakens the FM stability.

For the type A AFM ordering, the e_g-e_g orbital hopping is forbidden along the c-axis. Therefore, throughout the Q_3-Q_2 plane, the net gain in the band energy is weaker in comparison to the FM case. In this case, the competition between the JT energy and band energy lead to two global minima located at Q_3 = -0.18 Å and Q_2 = ± 0.32Å (see Fig. 5 (top right)) which is close to earlier experimental and theoretical studies[8,22,29]. In fact, taking the super exchange into account, these minima have the lowest energy in the Q_3-Q_2 plane when all the magnetic configurations are considered.

In the case of type C magnetic ordering, where the antiferromagnetic *ab* planes are stacked ferromagnetically along the *c*-axis, the hopping between the z^2-1 orbitals along the *c*-axis is only allowed and the remaining hopping interactions are forbidden either due to orbital symmetry along the *c*-axis or due to the Anderson-Hasegawa cos$(\theta/2)$ factor along the plane. As a result, the system gains very little band energy, making this phase unfavorable for all strains.

Total energy – The total energies of the various structures as a function of strain are plotted in Fig. 6. It is easy to understand several general features of the energy. First, note that with the energy minimum occurring at zero strain condition ($\varepsilon_{zz}=0$), the total energy is internally consistent. If the minimum occurred somewhere else, that would indicate that LMO would automatically occur with a different strain condition. The energy of the F structure does approach the minimum of the A structure at $\varepsilon_{zz}=0$, but does not come below it.

A second feature of the total energy is that for large strains, the octahedral distortion is strong, which leads to a large on-site splitting of the e_g states,

$$\epsilon_\pm = g'Q_1 \pm g\sqrt{Q_2^2+Q_3^2}, \tag{8}$$

the lower orbital being fully occupied and the higher orbital empty. This in turn leads to a vanishing gain in

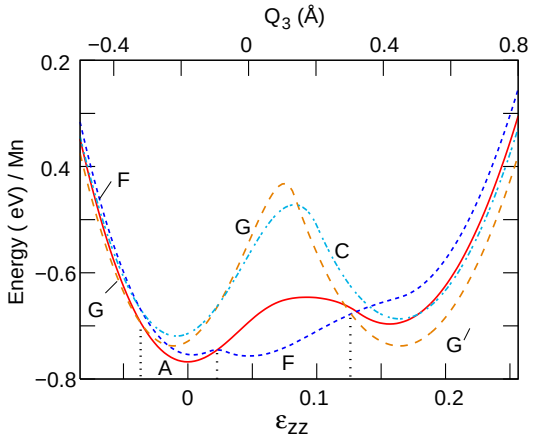

FIG. 6: (Color online) Total energy for the different phases as a function of strain. Parameters are the same as in Fig. 5.

energy due to hopping between the occupied and the unoccupied states because of the large energy denominator in the second order perturbation theory, irrespective of the magnetic structure and the corresponding Anderson-Hasegawa $\cos(\theta/2)$ factors. The net result is that for large strains, the energies for all structures simply tend to a sum of the elastic energy and the on-site JT energy:

$$E = (1/2)KQ^2 + g'Q_1 - g\sqrt{Q_2^2 + Q_3^2}. \qquad (9)$$

The quadratic dependence on the JT distortion or, equivalently, the strain for large strain for all magnetic structures is clearly seen in Fig. 6. The curves are parabolas with shifted minima for the G and G′ structures, where the expression (9) is exact, since there is no hopping for these structures. For the remaining structures, there is a gain of energy due to hopping, being maximum for the ferromagnetic F structure, where hopping is allowed in all directions in the lattice. This leads to the stability of the F structure for small strain parameters as seen from the figure. The argument is consistent with the fact that the energy gain for small strain progressively increases from C to A to F (as seen in Fig. 6), where hopping is allowed along one, two, and three directions, respectively, for these structures.

Another point regarding the total energy of Fig. 6 is that the ferromagnetic phase is always close by in energy for small strain situations, which is suggestive of the reason why LMO thin films are usually observed to occur in the ferromagnetic phase, rather than the A phase of the bulk.

Finally, one might ask how is it possible that at larger strains the Néel ordered G or G′ state wins over the ferromagnetic F state. The reason is that as strain is increased, the progressively larger JT distortions split the e_g states more and more (Eq. 8). The kinetic energy gain in the FM phase due to hopping between the occupied e_g state and the neighboring unoccupied e_g states progressively diminishes, due to the energy denominator in the second-order perturbation theory. This can not overcome the super exchange energy cost, so that the Néel ordered states win in the limit of large strains.

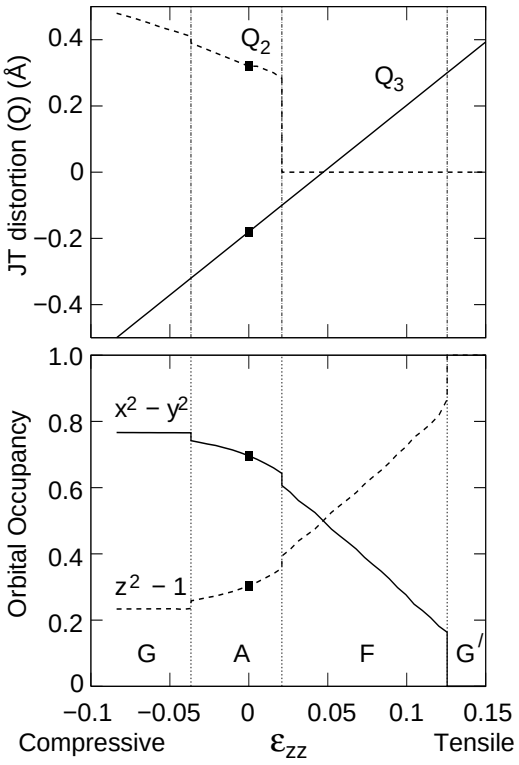

FIG. 7: Variation of the JT distortions (upper panel) and the occupancy of the Mn e_g orbitals (lower panel) as a function of the applied strain. In our model, Q_3 and ε_{zz} are linearly related by Eq. (6). The hopping parameter is V_σ = -0.5 eV. Dots denote the unstrained structure.

JT distortions and orbital occupancy – Turning now to the question of JT distortion strengths, Fig. 7 shows the variation of Q_2 and Q_3 modes and the change in the orbital occupancy as a function of strain. As discussed earlier, the Q_3 mode is directly related linearly to ε_{zz} through Eq. (6). Quite interestingly, we find that the magnitude of the in-plane distortion Q_2 at first diminishes and then sharply drops to zero as the strain is changed from compressive to tensile. This is due to the fact that in the compressive strain condition, the system stabilizes in the type G AFM ordering where the Q_2 mode is more favorable (see Fig. 4). On the other hand, in the tensile strain condition, in the stable ferromagnetic (F) ordering, kinetic energy gain is maximum if the e_g orbitals are not split, so that the JT distortion is small or non-existent.

Strain has a strong effect on the e_g orbital occupancies as indicated in Fig. 5. The calculated orbital occupancies are plotted in Fig. 7. In the A phase, the $x^2 - y^2$ and the z^2-1 orbitals add up with the proper linear combination to yield the checkerboard $x^2 - 1/y^2 - 1$ orbital ordering on alternate Mn atoms in the ab plane. As the strain

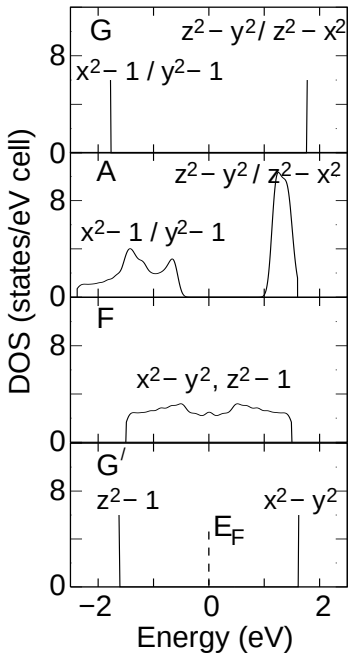

FIG. 8: Densities of states (DOS) corresponding to the four strain conditions of Fig. 2, with hopping parameter V_σ = -0.5 eV. In the Neél ordered G and G′ phases, complete suppression of hopping leads to the δ-functions in the DOS; In the G phase, alternate Mn sites have the x^2-1 or the y^2-1 orbitals occupied with the remaining component of the e_g manifold empty, leading to the checkerboard orbital ordering, while in the G′ phase, all sites have the z^2-1 orbital occupied. In the A phase, allowed hopping in the plane leads to a broadening of the band, but still a gap in the DOS remains. In the ferromagnetic F phase, hopping both in and out of the plane is strong enough to close the gap, leading to a metallic state due to band gap closure. The Fermi energy is taken as the zero of energy in this plot.

is increased, the z^2-1 orbital becomes more and more occupied with the occupancy becoming one in the G′ phase. This is because in this limit Q_3 is large and Q_2 is zero, so that the elongated Mn-O bond along the c-axis results in a strong octahedral crystal field that increases the energy of x^2-y^2 orbital, simultaneously lowering that of z^2-1 orbital and fully occupying it in the process. This physics is of course incorporated in the linear Jahn-Teller coupling term in our model Hamiltonian Eq. (3).

Beside the magnetic transitions, the other important feature in the strain induced LMO is a metal-insulator transition due to band gap closure. Fig. 8 shows the densities of states for the various phases, which faithfully indicates the strong JT splitting of the on-site energies of the e_g orbitals, $\Delta = g\sqrt{Q_2^2+Q_3^2}$, with only a large hopping in the ferromagnetic phase being able to close the gap and produce a metallic phase. In Fig. 9, we have shown the calculated band gap as a function of strain. We see that the gap changes abruptly as new phases are entered. We note that for the unstrained case, the magnitude of the band gap obtained with our parameters is

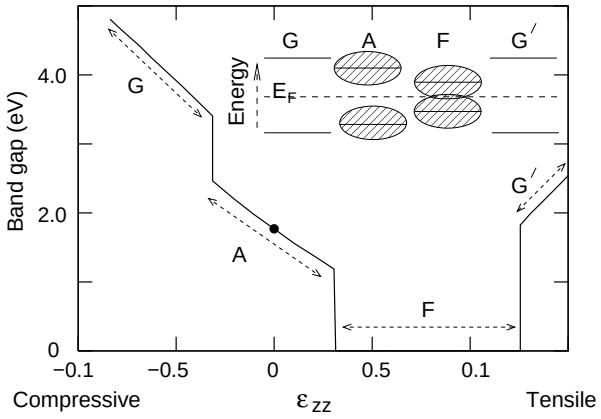

FIG. 9: Variation of the band gap with strain. Inset shows the typical band structure for the four phases. The black dot indicates the band gap for the unstrained LMO.

1.76 eV as compared to the measured value of 1.8 eV, obtained from the photoemission data[40]. This suggests that the experimental band gap under strain may also show changes similar to what is indicated from our model.

IV. SUMMARY

In summary, we studied the effect of uniaxial strain on the ground-state structure of $LaMnO_3$ from a model Hamiltonian that included the key interactions in the system, viz., the super exchange, the double exchange, and the Jahn-Teller electron-lattice coupling. Our results reveal the existence of various phases under varying strain conditions, where the orbital order, magnetic structure, octahedral JT distortions, as well as the conduction properties change under applied strain. Only the ferromagnetic phase, stable with a small tensile strain in our model, was found to be metallic, while all other phases were found to be insulating. The analysis presented here should be helpful in the interpretation of experiments on epitaxially grown $LaMnO_3$ heterostructures, which are often in the uniaxial strain condition.

This work was supported by the U. S. Department of Energy through Grant No. DE-FG02-00ER45818.

[1] C. Christides, P. P. Deen, N. Moutis, E. Houssakou, L. Bouchenoire, and K. Prassides, Phys. Rev. B 75, 014432 (2007).
[2] H. Yamada, M. Kawasaki, T. Lottermoser, T. Arima, and

Y. Tokura, Appl. Phys. Lett. **89**, 052506 (2006).
[3] T. Koida, M. Lippmaa, T. Fukumura, K. Itaka, Y. Matsumoto, M. Kawasaki, and H. Koinuma, Phys. Rev. B **66**, 144418 (2002).
[4] T. Satoh, K. Miyano, Y. Ogimoto, H. Tamaru, and S. Ishihara, Phys. Rev. B **72**, 224403 (2005).
[5] Ş. Smadici, P. Abbamonte, A. Bhattacharya, X. Zhai, B. Jiang, A. Rusydi, J. N. Eckstein, S. D. Bader, and J. M. Zuo, Phys. Rev. Lett. **99**, 196404 (2007).
[6] B. R. K. Nanda and S. Satpathy, Phys. Rev. Lett **101**, 127201 (2008).
[7] A. Y. Ramos, H. C. N. Tolentino, N. M. Souza-Neto, J. -P. Itié, L. Morales, and A. Caneiro, Phys. Rev. B **75**, 052103 (2007).
[8] I. Loa, P. Adler, A. Grzechnik, K. Syassen, U. Schwarz, M. Hanfland, G. Kh. Rozenberg, P. Gorodetsky, and M. P. Pasternak, Phys. Rev. Lett. **87**, 125501 (2001).
[9] L. P. Gaudart, J. R. Carvajal, A. D. Aladine, I. Goncharenko, M. Medarde, R. I. Smith, and A. Revcolevschi, Phys. Rev. B **64**, 064426 (2001).
[10] Y. Ding, D. Haskel, Y. -C. Tseng, E. Kaneshita, M. van Veenendaal, J. F. Mitchell, S. V. Sinogeikin, V. Prakapenka, and H. K. Mao, Phys. Rev. Lett. **102**, 237201 (2009).
[11] A. Tebano, C. Aruta, S. Sanna, P. G. Medaglia, and G. Balestrino, A. A. Sidorenko, R. De Renzi, G. Ghiringhelli, L. Braicovich, V. Bisogni, and N. B. Brookes Phys. Rev. Lett. **100**, 137401 (2008); C. Aruta, G. Ghiringhelli, A. Tebano, N. G. Boggio, N. B. Brookes, P. G. Medaglia, and G. Balestrino, Phys. Rev. B **73**, 235121 (2006); A. Tebano, A. Orsini, P.G. Medaglia, and G. Balestrino, Appl. Phys. Lett. **94**, 242503 (2009).
[12] Y. Konishi, Z. Fang, M. Izumi, T. Manako, M. Kasai, H. Kuwahara, M. Kawasaki, K. Terakura, and Y. Tokura, J. Phys. Soc. Jpn, **68**, 3790 (1999).
[13] J. Zhang, H. Tanaka, T. Kanki, J -H. Choi, and T. Kawai, Phys. Rev. B **64**, 184404 (2001).
[14] J. H. Song, J. H. Park, K. -B. Lee, J. M. Lee, and Y. H. Jeong, Phys. Rev. B **66**, 020407(R) (2002).
[15] A. Dubey, V. G. Sathe, and R. Rawat, J. Appl. Phys. **104**, 113530 (2008).
[16] Y. Suzuki, H. Y. Hwang, S-W. Cheong, and R. B. van Dover, Appl. Phys. Lett. **71**, 140 (1997).
[17] J. Z. Sun, D. W. Abraham, R. A. Rao, and C. B. Eom, Appl. Phys. Lett. **74**, 3017 (1999).
[18] H. Meskine, H. König, and S. Satpathy, Phys. Rev. B **64**, 094433 (2001).
[19] B. R. K. Nanda and S. Satpathy, Phys. Rev. B **79**, 054428 (2009).
[20] B. R. K. Nanda and S. Satpathy, Phys. Rev. B **78**, 054427 (2008).
[21] S. Satpathy, Z. S. Popović, and F. R. Vukajlović, Phys. Rev. Lett. **76**, 960 (1996).
[22] D. J. Singh and W. E. Pickett, Phys. Rev. B **57**, 88 (1998).
[23] W. E. Pickett and D. J. Singh, Phys. Rev. B **53** 1146 (1996).
[24] H. Zenia, G. A. Gehring, W. M. Temmerman, New J. Physics **7** 257 (2005).
[25] G. Trimarchi and N. Binggeli, Phys. Rev. B **71**, 035101 (2005).
[26] A. Yamasaki, M. Feldbacher, Y. -F. Yang, O. K. Andersen, and K. Held, Phys. Rev. Lett. **96**, 166401 (2006).
[27] B. R. K. Nanda and S. Satpathy (To be published).
[28] J. Kanamori, J. Appl. Phys. Suppl. **31**, 14S (1960).
[29] Z. Popović and S. Satpathy, Phys. Rev. Lett. **84**, 1603 (2000).
[30] C. Zener, Phys. Rev. **82**, 403 (1951).
[31] P. W. Anderson and H. Hasegawa, Phys. Rev. **100**, 675 (1955).
[32] W. A. Harrison, *Electronic Structure and the Properties of Solids* (Freeman, San Francisco, 1979).
[33] A. J. Millis, Phys. Rev. B **53**, 8434 (1996).
[34] E. O. Wollan and W. C. Koehler, Phys. Rev. **100**, 545 (1955).
[35] G. S. Rushbroke, G. S. Baker, Jr. and P. J. Wood, in *Phase Transitions and Critical Phenomena, edited by* C. Domb and M. S. Green (Academic Press, London, New York, 1974), Vol. 3, Eqs. (1.1) and (5.4).
[36] J. B. A. A. Elemans, B. van Laar, K. R. van der Veen, and B. O. Loopstra, J. Solid State Chem. **3**, 238 (1971).
[37] C. Adamo, X. Ke, H. Q. Wang, H. L. Xin, T. Heeg, M. E. Hawley, W. Zander, J. Schubert, P. Schiffer, D. A. Muller, L. Maritato, and D. G. Scholm, Appl. Phys. Lett. **95**, 112504 (2009)
[38] H. R. Salva, A. A. Ghilarducci, A. G. Leyva, and S. S. Seiro, J. Mag. Mag. Mat. **310**, e626 (2007).
[39] I. B. Bersuker, *The Jahn-Teller Effect and Vibronic Interactions in Modern Chemistry* (Plenum Press, New York, 1984).
[40] T. E. Saitoh, A. E. Bocquet, T. Mizokawa, H. Namatame, A. Fujimori, M. Abbate, Y. Takeda, and M. Takano, Phys. Rev. B **51** 13942 (1995).